Communication

Dual-Band Antenna With Pattern and Polarization Diversity

Jungmin Mo and Youngje Sung *

Posted Date: 5 July 2024

doi: 10.20944/preprints202407.0470.v1

Keywords: High isolation; Pattern-diversity antenna; Polarization diversity

Communication

Dual-Band Antenna with Pattern and Polarization Diversity

Jungmin Mo and Youngje Sung *

Department of Electronic Engineering, Kyonggi University, Suwon 16227, Republic of Korea; mojung0725@kyonggi.ac.kr
* Correspondence: yjsung@kyonggi.ac.kr

Abstract: In this letter, we propose a pattern-diversity antenna with different radiation patterns at two different frequency bands (f_1 and f_2) (f_1: broadside radiation pattern, f_2: conical radiation pattern). The proposed structure consists of a central circular antenna and two annular ring antennas; each of the three antennas has individual ports. Two of the ports exhibit orthogonal broadside radiation patterns; the other two ports exhibit orthogonal conical radiation patterns. Thus, they have polarization diversity characteristics. To improve isolation between ports, the inner part of the annular ring antennas is shorted via array, and the outermost port is positioned orthogonal to the other ports. Using this configuration, the isolation between ports was measured as -26.7 dB and -30.1 dB at the two frequency bands, respectively. Experimental results based on the fabricated prototype show that the proposed antenna achieves -10 dB bandwidths of 240 MHz (5.71~5.95 GHz) and 210 MHz (7.69~7.9 GHz) at f_1 and f_2, respectively.

Keywords: high isolation; pattern-diversity antenna; polarization diversity

1. Introduction

Dual-Band antennas enable simultaneous use of two communication links with a single antenna. Additionally, when applied to GPS systems, dual-band technology can provide improved accuracy compared to using a single frequency. By incorporating additional frequency bands, dual-band antennas can enhance data quality and connection success rates, overcoming the limitations of using a single frequency band [1].

There are two main methods for implementing dual-band antennas. One approach involves positioning two or more independent antennas closely together to create a dual-band antenna [2,3] another method is to use a single antenna [4–7]. The former method of placing multiple independent antennas adjacent to each other is becoming less popular due to the relatively large size. Dual-band antennas with a single resonator use substrate-integrated waveguide (SIW) technology [4,5] or using diplexing methods [6,7]. These methods share the same structure and can be seamlessly integrated into a common design. However, the frequency ratio is small.

A radiation pattern indicates the directionality and strength of the signal being transmitted. Antennas have their own unique radiation patterns; a radiation pattern is selected based on the usage requirements. Radiation pattern diversity is a key technology in systems such as multiple-input–multiple-output (MIMO) antennas. Using different radiation patterns, we can increase data transmission rates, mitigate interference, and minimize the impact of multipath effects [8].

Many studies have implemented radiation-pattern diversity. A single port can be used to obtain different radiation patterns at multiple frequency bands. This has been achieved using antennas based on artificial magnetic conductors (AMCs) [9] or applying spiral inverted-F antennas [10]. Multiple ports at specific frequencies can be used to achieve different radiation patterns. Given isolation between ports, methods that arrange ports vertically [12] or use annular ring antennas with shorted inner parts have been used [13]. Furthermore, combination of inductive loaded patches and annular ring antennas has been used to diversify radiation patterns and polarization [14]. Multiple ports at different frequency bands can be used to obtain different radiation patterns. This can be achieved by aligning the centers of circular antennas and annular ring antennas [15]. In another method, a sequentially rotated microstrip feed is used for the high band and four open-ended slots are used for an omni-directional pattern in the low band [16]. Shielded mushroom structures in artificial transmission lines (ATLs) have been used to implement dual-band triple-mode antennas [17].

In this research, we achieved dual-band characteristics using a circular antenna and an annular ring antenna with its inner part shorted via an array. We obtained two different radiation patterns at two frequency bands and simultaneously obtained identical but orthogonal radiation patterns at the same frequency band. In Table I, we compare the performance of the proposed antenna with previously published dual-band microstrip

 doi:10.20944/preprints202407.0470.v1

antennas. The presented metrics are simulation results obtained using HFSS. The measured data were obtained through experiments conducted with fabricated prototypes.

Table 1. Comparison with previous dual-feed dual-cp antennas.

Ref.	Freq. [GHz]	BW [%]	Size	# of port	Iso. [dB]	Pattern
[2]	5.8/ 30	3.1/ 8.1 17/ 6.3	$1.90\lambda_0 \times 1.90\lambda_0 \times 0.020\lambda_0$	2	< -25	O/ B
[4]	5.2/ 5.8	6/ 3.4	$1.50\lambda_0 \times 1.30\lambda_0 \times 0.038\lambda_0$	2	-28	B/ B
[5]	8.3/ 10.5	1.9/ 2.7	$0.88\lambda_0 \times 0.72\lambda_0 \times 0.040\lambda_0$	2	-27.9	B/ B
[6]	2.5/ 5.3	4.5/ 5.5	$0.57\lambda_0 \times 0.57\lambda_0 \times 0.010\lambda_0$	2	-21	B/ B
[7]	2.5/ 5.5	1.3/ 3	$0.20\lambda_0 \times 0.10\lambda_0 \times 0.014\lambda_0$	2	-26	O/ O
[9]	1.4/ 1.6	2/ 1	$0.57\lambda_0 \times 0.57\lambda_0 \times 0.030\lambda_0$	1	X	O/ B
[10]	2.5/ 5.8	4/ 3.4	$0.30\lambda_0 \times 0.30\lambda_0 \times 0.080\lambda_0$	1	X	O/ B
[12]	3.5	1.4	$0.35\lambda_0 \times 0.35\lambda_0 \times 0.035\lambda_0$	3	$-13/ -13/ -25$	O/ B/ B
[13]	5.8	2.5	$0.96\lambda_0 \times 0.96\lambda_0 \times 0.030\lambda_0$	2	-26.5	O / B
[15]	2.4/ 5.8	0.9/ 2 2/ 1.8	$0.28\lambda_0 \times 0.28\lambda_0 \times 0.012\lambda_0$	2	< -26	O/ B
[16]	2.5/ 5.9	8.1/ 10.3	$0.40\lambda_0 \times 0.40\lambda_0 \times 0.035\lambda_0$	2	$-14/ -16$	O/ B
[18]	2.5/ 3.5	1/ 1.6 6.7/ 1.2	$0.90\lambda_0 \times 0.90\lambda_0 \times 0.060\lambda_0$	2	$-25.4/ -22.3$	B/ O
This work	5.9/ 7.9	3.6/ 3.6 1.5/ 2.1	$0.49\lambda_0 \times 0.49\lambda_0 \times 0.030\lambda_0$	3	$-26.7/ -30.1$	B/O

2. Antenna Configuration

Figure 1 shows the configuration of the proposed antenna. The substrate used in the design is RO4003C with a thickness of 1.58 mm, a dielectric constant of 3.55, and a loss tangent of 0.0027. The proposed antenna consists of one circular antenna and two annular ring antennas shorted via an array. The radii of the vias located inside are 0.27 mm; the radii of the vias located outside are 0.6 mm. The outermost ring antenna (Antenna I), has outer and inner radii denoted as r_1 and r_2, respectively. Antenna II is positioned with outer and inner radii denoted as r_3 and r_4, respectively. In the center, there is a circular antenna with a radius of r_5 (Antenna III). The ground radius is set to r_0. The positions of the ports are determined by d_1, d_2, and d_3.

Antennas 2 and 3 are positioned inside the ring structure of Antenna I, allowing the antennas to achieve different radiation patterns (broadside radiation pattern and conical radiation pattern) at two different frequency bands without increasing the size of the antenna. To enhance isolation between ports, vias are incorporated into the structure; Antenna I has 30 vias and Antenna II has 60 vias. Antennas 1 and 3 form a broadside radiation pattern at 5.93 GHz in the TM_{11} mode; Antennas 1 and 2 form a conical radiation pattern at 7.92 GHz in the TM_{41} and TM_{21} modes, respectively. Port 1 is positioned orthogonal to Ports 2 and 3 for good isolation. Furthermore, the vias located on the outer side improve the isolation characteristics between antennas.

 doi:10.20944/preprints202407.0470.v1

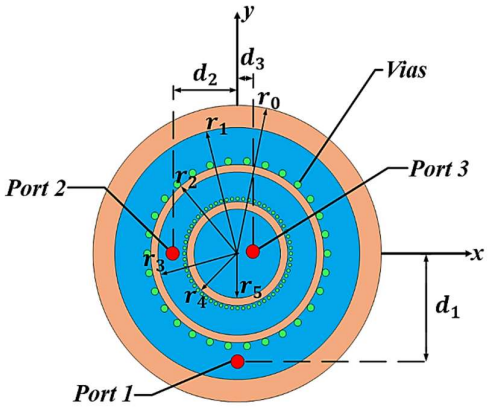

Figure 1. Geometry of the proposed antenna.

The resonant frequencies of the TM modes of the proposed antennas can be determined using (1) [19,20].

$$f_{nm} = \frac{X_{nm}c}{2\pi a_e\sqrt{\varepsilon_r}} \quad (1)$$

In this equation, *nm* is related to the TM_{nm} mode; *c* represents the speed of light, and ε_r denotes the dielectric constant of the substrate. a_e denotes the effective radius, which can be obtained using (2). X_{nm} is the root of (3); its values are X_{11}=1.8412, X_{21}=1.3406, and X_{41}=2.5876 [21].

In (2), *a* represents the radius for a circular antenna and the inner radius for a ring antenna; *h* denotes the height of the substrate. Equation (3) is derived from the boundary conditions of the cavity mode for these antennas. Here, *g* is the ratio of the outer radius to the inner radius, and J_n and N_n denote the n^{th} order Bessel functions of the first and second kind, respectively, where the prime notation indicates the first derivative.

$$a_e = a\sqrt{1 + \frac{2h}{\pi a\varepsilon_r}\left(ln\frac{\pi a}{2h} + 1.776\right)} \quad (2)$$

$$J'_{nm}(k_{nm})N_n(k_{nm}g) - J_n(k_{nm}g)N'_{nm}(k_{nm}) = 0 \quad (3)$$

3. Parameter Study

A. Isolation Based on Port Positions

Figure 2(a) shows the antenna configurations corresponding to different port positions. Antenna I shows three ports aligned in a straight line. Antenna II shows a 90° rotation of port 2. Antenna III shows a 90° rotation of port 1. Antenna IV shows a 90° rotation of ports 1 and 2. The antenna parameters except for the port positions are set as follows. The antenna dimensions are: r_0 = 25 mm, r_1 = 21.5 mm, r_2 = 15 mm, r_3 = 13.97 mm, r_4 = 8.75 mm, r_5 = 7.45 mm. The radius of the via for Antenna I is 0.6 mm, and for Antenna II is 0.27 mm. The positions of the three ports in the proposed structure are set as follows: d_1 = 18.4 mm, d_2 = 10.78 mm, d_3=2.3 mm. Figure 2(b) presents the simulation results for isolation as the antenna ports are rotated by 90°. Figure 2(c) and 2(d) show the simulation results for isolation at frequencies of 5.93 GHz and 7.92 GHz, respectively. From the simulation results, when port 1 and port 3 are perpendicular to each other, the isolation characteristics are good.

In Figure 2(c), the isolation between port 1 and port 3 of each model at the 5.9 GHz band is -13 dB (Antennas I and II, where the two ports are horizontal). In comparison, Antennas III and IV, where the two ports are perpendicular, show an improved isolation of approximately -30 dB. Port 2 does not significantly influence the isolation characteristics based on its position relative to the other two ports. In Figure 2(d), comparing the S_{21} at 7.92 GHz, all three antenna models exhibit isolation values of approximately -30 dB. Based on these results, Antenna III was selected to enhance the isolation characteristics between the antenna ports.

 doi:10.20944/preprints202407.0470.v1

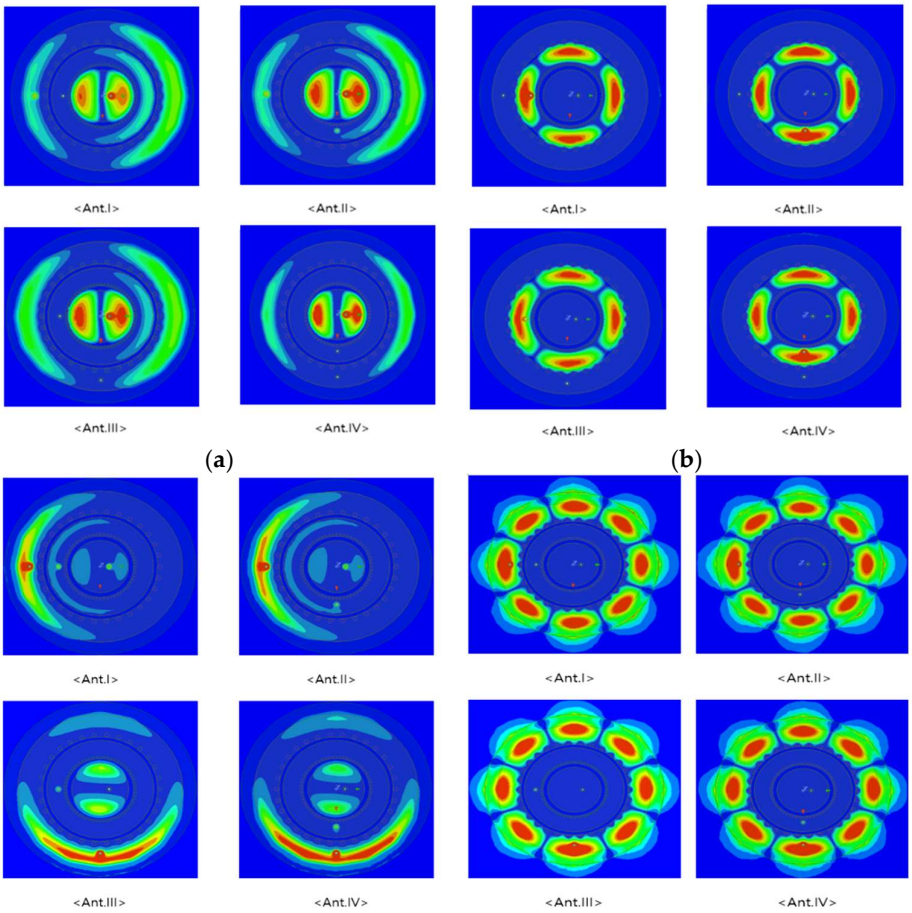

Figure 2. E-field distribution: (a) at 5.93 GHz_port1; (b) at 7.92 GHz_port1; (c) at 5.93 GHz_port3; (d) at 7.92 GHz_port2. .

B. Effect of Number of Vias

According to [22], adjusting the number of vias in the antenna can control the resonant frequencies corresponding to each TM mode and can adjust the bandwidth or separate the bands.

Figure 3(a) shows the simulation results with different reflection coefficients based on the number of vias located on Antenna I to observe the change in the angle between the vias. The angle between the vias was set to 5°, 12°, and 15°; all other antenna parameters were kept constant. From Figure 3, there is not a significant difference in performance based on the number of vias in S_{33}. However, for S_{11}, as the angle between the vias increases (with fewer vias), the resonant frequency decreases, indicated by the green diamonds in Figure 3(a). With an angle of 12°, there is a wider bandwidth below -10 dB than with angles of 5° and 15°. For S_{22}, it is also evident that a 12° angle provides the widest bandwidth below -10 dB. Based on these results, the angle between the vias was set to 12°.

Preprints.org (www.preprints.org) | NOT PEER-REVIEWED | Posted: 5 July 2024 doi:10.20944/preprints202407.0470.v1

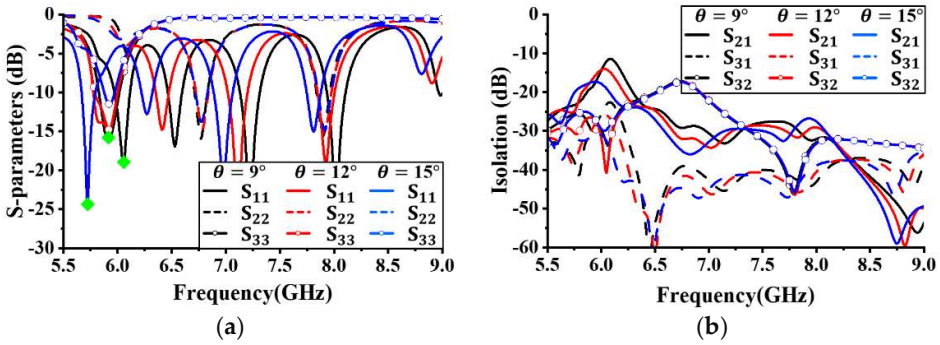

(a) (b)

Figure 3. Simulated antenna performance with different angels(θ) between the vias: (a) Reflection Coefficient; (b) Isolation.

C. Effect of Antenna Size

Figure 4 shows the simulation results for reflection coefficients and isolation characteristics with different lengths r_1. The length of r_1 was increased from 21 mm in 0.5-mm increments; all other antenna parameters were kept constant. In Figure 4(a), it is observed that there is no significant performance difference in S_{22} with changes in the size of r_1. However, for S_{11}, as r_1 increases (as the size of Antenna I increases), the resonant frequency decreases, as indicated by the green diamonds in Figure 4(a). For S_{33}, there is no bandwidth below -10 dB with a size of 21 mm; with a size of 22 mm, the bandwidth is much narrower than with a size of 21.5 mm. Based on these results, the radius r_1 of Antenna I was set to 21.5 mm.

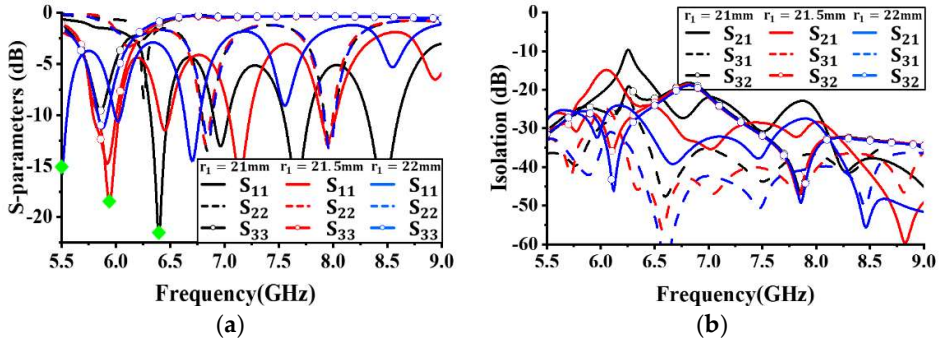

(a) (b)

Figure 4. Simulated antenna performance with different radius r_1: (a) Reflection coefficient; (b) Isolation.

Figure 5 shows the simulation results for reflection coefficients and isolation characteristics with different values of r_3. The length of r_3 was increased from 13.8 mm in 0.1-mm increments; all other antenna parameters were kept constant. In Figure 5(a), it is observed that r_3 does not have a significant effect on S_{11} and S_{33}. However, for S_{22}, as r_3 increases (as the size of Antenna II increases), the resonant frequency decreases, indicated by the green diamonds in Figure 5(a). Based on these results, the radius r_3 was set to 13.97 mm and the isolation values for each operating band were all below -20 dB.

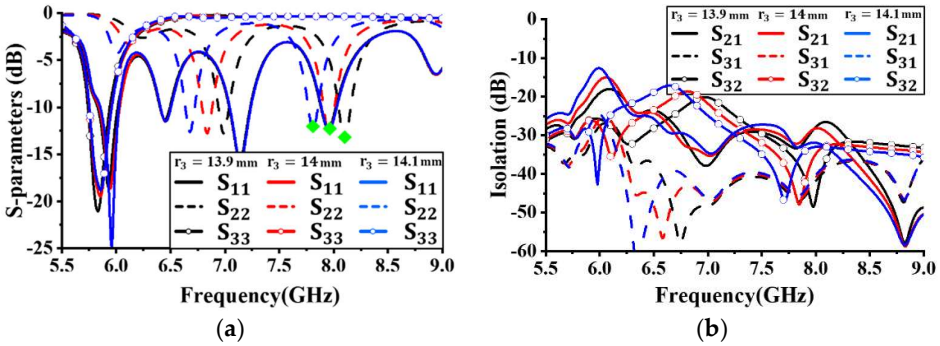

(a) (b)

Figure 5. Simulated antenna performance with different radius r_3: (a) Reflection coefficient; (b) Isolation.

 doi:10.20944/preprints202407.0470.v1

Figure 6 shows the simulation results for reflection coefficients and isolation characteristics with different values of r_5. r_5 was increased from 7.25 mm in 0.2-mm increments; all other antenna parameters were kept constant. In Figure 6(a), it is observed that there is no significant performance difference in S_{22} with changes in the size of r_5. Although there are some variations in the resonant frequency and reflection coefficient values for S_{11}, they are not significant. However, for S_{33}, as r_5 increases, the resonant frequency decreases, indicated by the green diamonds in Figure 6(a). Additionally, the bandwidth below -10 dB was widest when the size was 7.45 mm. Based on these results, the radius r_3 was set to 13.9 mm. At this size, the isolation values for each operating band were all below -20 dB.

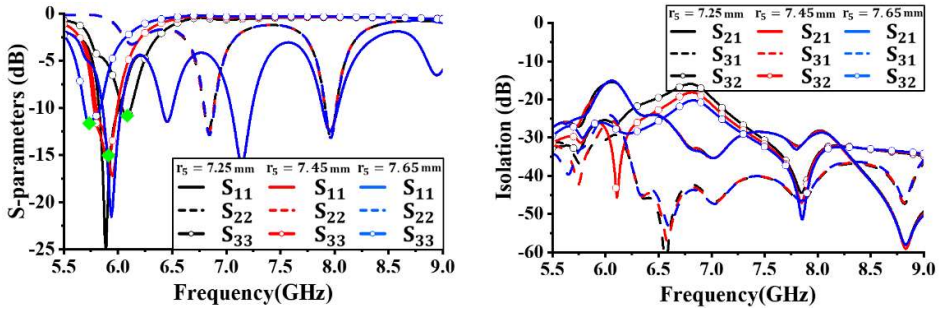

Figure 6. Simulated antenna performance with different radius r_5: (a) Reflection coefficient; (b) Isolation.

4. Simulated and Measured Results

Figure 7 shows a photograph of the proposed antenna, fabricated using the optimized parameters. Figure 8 compares the simulated and measured reflection coefficients and isolation characteristics of the proposed antenna. The bandwidth of -10 dB for the two frequency bands is shown in Figure 8(a). For f_1, the common bandwidth between port 1 and port 3 is from 5.71–5.95 GHz, resulting in a bandwidth of 210 MHz. Figure 8(b) shows the isolation characteristics for the ports at each resonant frequency. The isolation between port 1 and port 2 is approximately -35.5 dB. The measured results also confirm good isolation between the ports. The resonant frequencies were shifted approximately 150 MHz lower than the simulated results. This discrepancy was caused by slight variations in the patch antenna dimensions during fabrication.

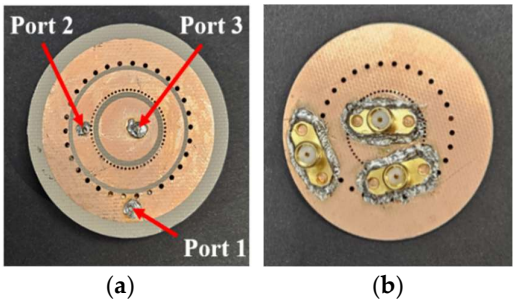

Figure 7. Prototype of the proposed antenna: (a) Top layer; (b)Bottom layer.

Preprints.org (www.preprints.org) | NOT PEER-REVIEWED | Posted: 5 July 2024 doi:10.20944/preprints202407.0470.v1

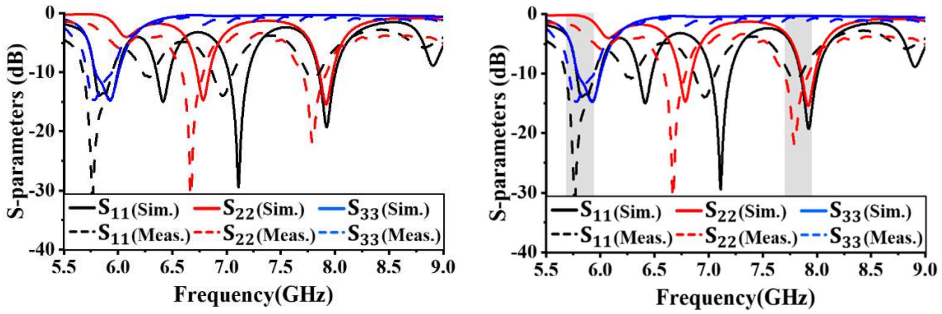

Figure 8. Simulated and measured results: (a) Reflection coefficient; (b) Isolation.

Figure 9 shows the electric field formed on the antenna surface as RF power is applied to different ports at resonant frequencies. The regions closer to red indicate stronger electric fields; regions closer to blue indicate weaker fields. Figure 9(a) shows the simulation results for the E-field when RF power is applied to port 1 at 5.93 GHz. The electric field along the horizontal axis where port 3 is located becomes null, indicating that the ports do not influence each other. Similarly, Figure 9(b) shows the simulation results when power is applied to port 3 at 5.93 GHz. The electric field along the vertical axis where port 1 is located becomes null, indicating no influence between the ports. As shown in Figure 9(c) and 9(d), the electric field is very weak at ports other than the one where power is applied, indicating no influence. Based on the simulation results, it can be concluded that the proposed antenna exhibits excellent isolation characteristics.

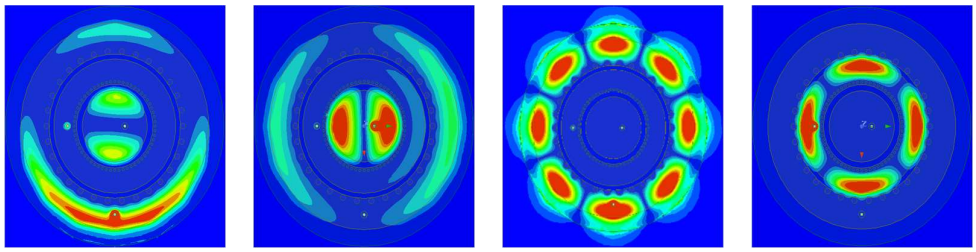

Figure 9. Simulated E-field distribution: (a) 5.93 GHz @ port 1; (b) 5.93 GHz @ port 3; (c) 7.92 GHz @ port 1; (d) 7.92 GHz @ port 2.

Figure 10 compares the measured radiation patterns of the proposed antenna with the simulated results. In Figure 10(a) and 10(b), at 5.93 GHz, broadside patterns are formed at ports 1 and 3, with energy radiated in the +z-axis direction. At 7.92 GHz, conical patterns are formed at ports 1 and 2, as shown in Figure 11(a) and 11(b). The measured results closely match the simulated values, indicating similar characteristics. The measured antenna gains are approximately 8.2 dBi for port 1 and 8.8 dBi for port 3 at 5.93 GHz. At 7.92 GHz, the gains are approximately 4.9 dBi for port 1 and 6.9 dBi for port 2.

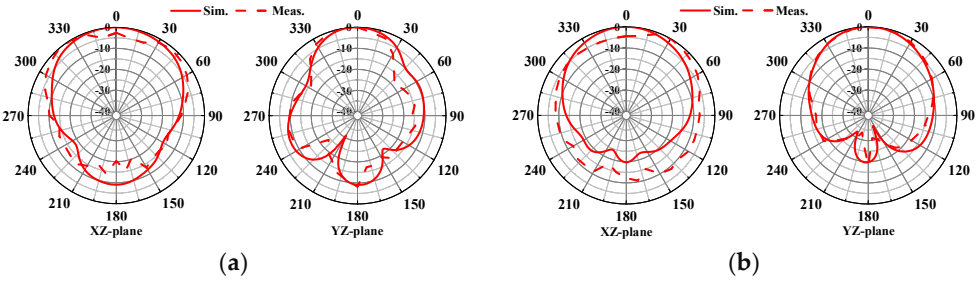

Figure 10. Normalized radiation pattern at 5.93 GHz: (a) port 1; (b) port 3.

 doi:10.20944/preprints202407.0470.v1

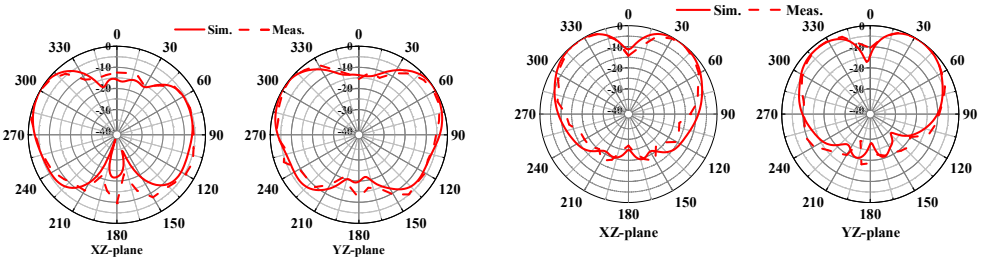

(**a**) (**b**)

Figure 11. Normalized radiation pattern at 7.92 GHz: (a) port 1; (b) port 2.

5. Conclusions

In this letter, we propose an antenna with both pattern and polarization diversity. We implement a pattern-diversity antenna with different radiation patterns in two different frequency bands. The proposed antenna consisted of one circular antenna and two ring antennas with the inner section shorted via an array. Each antenna used a feeding method using probes. To improve isolation between ports, each port was designed to be orthogonal. As a result, the isolation between ports was -26.7 dB and -30.1 dB at the two frequency bands, respectively. Based on its excellent isolation characteristics, the proposed antenna exhibits broadside radiation pattern characteristics at f_1 and conical radiation pattern characteristics at f_2, perpendicular to each other. Thus, we believe that the proposed antenna has potential for multi-band mobile communication applications.

References

1. S. V. Nandigama, B. Kunooru, D. Ramakrishna and V. M. Pandharipande, “Pattern similarity and gain enhancement of dual-band antenna using an ENZ metamaterial,” in Journal of Electromagnetic Engineering and Science, vol.23, no. 6, pp. 461-469, Nov. 2023.
2. B. J. Xiang, S. Y. Zheng, H. Wong, Y. M. Pan, K. X. Wang and M. H. Xia, "A flexible dual-band antenna with large frequency ratio and different radiation properties over the two bands," in *IEEE Transactions on Antennas and Propagation*, vol. 66, no. 2, pp. 657-667, Feb. 2018.
3. Y. Q. Guo, Y. M. Pan, S. Y. Zheng and K. Lu, "A singly-fed dual-band microstrip antenna for microwave and millimeter-wave applications in 5G wireless communication," in *IEEE Transactions on Vehicular Technology*, vol. 70, no. 6, pp. 5419-5430, June 2021.
4. D. Chaturvedi, A. Kumar and S. Raghavan, "A nested SIW cavity-backing antenna for Wi-Fi/ISM band applications," in *IEEE Transactions on Antennas and Propagation*, vol. 67, no. 4, pp. 2775-2780, April 2019.
5. S. Nandi and A. Mohan, "An SIW cavity-backed self-diplexing antenna," in *IEEE Antennas and Wireless Propagation Letters*, vol. 16, pp. 2708-2711, 2017.
6. Y. -J. Lee, J. -H. Tarng and S. -J. Chung, "A filtering diplexing antenna for dual-band operation with similar radiation patterns and low cross-polarization levels," in *IEEE Antennas and Wireless Propagation Letters*, vol. 16, pp. 58-61, 2017.
7. Y. -C. Lu and Y. -C. Lin, "A mode-based design method for dual-band and self-diplexing antennas using double T-stubs loaded aperture," in *IEEE Transactions on Antennas and Propagation*, vol. 60, no. 12, pp. 5596-5603, Dec. 2012.
8. M. S. Sharawi, "Printed multi-band MIMO antenna systems and their performance metrics [wireless corner]," in *IEEE Antennas and Propagation Magazine*, vol. 55, no. 5, pp. 218-232, Oct. 2013.
9. J. Lin, Z. Qian, W. Cao, S. Shi, Q. Wang and W. Zhong, "A low-profile dual-band dual-mode and dual-polarized antenna based on AMC," in *IEEE Antennas and Wireless Propagation Letters*, vol. 16, pp. 2473-2476, 2017.
10. X. Y. Zhang, H. Wong, T. Mo and Y. F. Cao, "Dual-band dual-mode button antenna for on-body and off-body communications," in *IEEE Transactions on Biomedical Circuits and Systems*, vol. 11, no. 4, pp. 933-941, Aug. 2017.
11. T. Zhang, W. Hong, Y. Zhang and K. Wu, "Design and analysis of SIW cavity backed dual-band antennas with a dual-mode triangular-ring slot," in *IEEE Transactions on Antennas and Propagation*, vol. 62, no. 10, pp. 5007-5016, Oct. 2014.
12. D. Piao and Y. Wang, "Tripolarized MIMO antenna using a compact single-layer microstrip patch," in *IEEE Transactions on Antennas and Propagation*, vol. 67, no. 3, pp. 1937-1940, March 2019.
13. S. Mirhadi, "Single-layer, dual-port, and dual-mode antenna with high isolation for WBAN Communications," in *IEEE Antennas and Wireless Propagation Letters*, vol. 21, no. 3, pp. 531-535, March 2022.
14. S. Yan and G. A. E. Vandenbosch, "Wearable antenna with tripolarization capability," *2017 International Workshop on Antenna Technology: Small Antennas, Innovative Structures, and Applications (iWAT)*, Athens, Greece, 2017, pp. 129-131.

 doi:10.20944/preprints202407.0470.v1

15. Z. G. Liu and Y. X. Guo, "Dual band low profile antenna for body centric communications," in *IEEE Transactions on Antennas and Propagation*, vol. 61, no. 4, pp. 2282-2285, April 2013.
16. C. -X. Mao, D. H. Werner, Y. Zhang and X. -Y. Zhang, "Compact dual-band dual-mode antenna with omni-/unidirectional radiation characteristics," in *IEEE Antennas and Wireless Propagation Letters*, vol. 18, no. 12, pp. 2657-2660, Dec. 2019.
17. K. Zhang, Z. H. Jiang, T. Yue, Y. Zhang, W. Hong and D. H. Werner, "A compact dual-band triple-mode antenna with pattern and polarization diversities enabled by shielded mushroom structures," in *IEEE Transactions on Antennas and Propagation*, vol. 69, no. 10, pp. 6229-6243, Oct. 2021.
18. S. Yan, J. Zhang, X. Hu and G. A. E. Vandenbosch, "Dual-band CRLH-TL based patch antenna with pattern diversity," *2017 11th European Conference on Antennas and Propagation (EUCAP)*, Paris, France, 2017, pp. 2956-2959.
19. I. Kaur *et al*., "Annular ring ultra wideband antenna integrated with metallic via array for IoT applications," in *IEEE Access*, vol. 10, pp. 73446-73457, 2022.
20. K. Y. Kapusuz, S. Lemey, A. Petrocchi, P. Demeester, D. Schreurs and H. Rogier, "Polarization reconfigurable air-filled substrate integrated waveguide cavity-backed slot antenna," in *IEEE Access*, vol. 7, pp. 102628-102643, 2019.
21. Garg, R., Bhartia, P., & Ittipiboon, A. (2001). Microstrip antenna design handbook. Boston (Mass.): Artech house, pp.317-324.
22. J. Liu, Q. Xue, H. Wong, H. W. Lai and Y. Long, "Design and analysis of a low-profile and broadband microstrip monopolar patch antenna," in IEEE Transactions on Antennas and Propagation, vol. 61, no. 1, pp. 11-18, Jan. 2013.